The radial evolution of solar wind speeds

S. L. McGregor,[1] W. J. Hughes,[1] C. N. Arge,[2] D. Odstrcil,[3] and N. A. Schwadron[4]

Received 10 August 2010; revised 30 November 2010; accepted 13 January 2011; published 31 March 2011.

[1] The WSA-ENLIL model predicts significant evolution of the solar wind speed. Along a flux tube the solar wind speed at 1.0 AU and beyond is found to be significantly altered from the solar wind speed in the outer corona at 0.1 AU, with most of the change occurring within a few tenths of an AU from the Sun. The evolution of the solar wind speed is most pronounced during solar minimum for solar wind with observed speeds at 1.0 AU between 400 and 500 km/s, while the fastest and slowest solar wind experiences little acceleration or deceleration. Solar wind ionic charge state observations made near 1.0 AU during solar minimum are found to be consistent with a large fraction of the intermediate-speed solar wind having been accelerated or decelerated from slower or faster speeds. This paper sets the groundwork for understanding the evolution of wind speed with distance, which is critical for interpreting the solar wind composition observations near Earth and throughout the inner heliosphere. We show from composition observations that the intermediate-speed solar wind (400–500 km/s) represents a mix of what was originally fast and slow solar wind, which implies a more bimodal solar wind in the corona than observed at 1.0 AU.

Citation: McGregor, S. L., W. J. Hughes, C. N. Arge, D. Odstrcil, and N. A. Schwadron (2011), The radial evolution of solar wind speeds, *J. Geophys. Res.*, *116*, A03106, doi:10.1029/2010JA016006.

1. Introduction

[2] It is generally agreed that the fast solar wind originates from coronal holes, and that the slow solar wind originates from somewhere else (e.g., active regions, coronal hole boundaries, streamer belts, quiet Sun, loops, etc.). In situ observations (e.g., FIP effect, helium abundance, charge state ratios) provide strong evidence that the fast solar wind originates from a different region of the solar corona than does the highly variable slow solar wind. With different compositions and coronal conditions it should be possible to learn something of the solar wind source regions. However, the solar wind structure evolves as it flows outward through the heliosphere away from the Sun. This complicates the problem, making it more difficult to definitively correlate in situ observations of the speed and composition and hence the source region of the solar wind. For example, during its second fast latitude scan Ulysses showed evidence of slow solar wind flows (<600 km/s) whose compositional signatures were consistent with fast flows from coronal holes, not slow solar wind [*McComas et al.*, 2002]. Solar wind models can help us understand this radial evolution of the solar wind speed, and shed some light on the compositional observations. The radial evolution of the solar wind speed is also important to understanding CME propagation as well as to mapping solar wind observations back to their photospheric origins.

[3] In this paper we analyze the radial evolution of the solar wind speed between 0.1 AU and 1.0 AU, using the combined Wang Sheeley Arge(WSA)-ENLIL solar wind model. We employ an inverse mapping technique, starting at 1.0 AU and following flows to their origin at the 21.5 solar radii (0.1 AU) inner boundary of ENLIL. We find a significant evolution of the solar wind speed, which occurs mainly in the first few tenths of an AU. This evolution is particularly prominent during solar minimum with the greatest evolution in solar wind speed occurring in solar wind with speeds at 1.0 AU of 400–500 km/s. During solar maximum the solar wind also undergoes significant speed evolution, but not as marked as during solar minimum. We find observational evidence of radial solar wind speed evolution using solar wind composition observations obtained during solar minimum when the models show the greatest evolution in the solar wind speed. Ionic charge states observed by the SWICS instrument on ACE are consistent with significant solar wind speed evolution between 0.1 AU and 1.0 AU.

2. Modeling

[4] We use the combined WSA-ENLIL model [*Odstrcil*, 2003; *Owens et al.*, 2008]. The WSA model is a coupled potential field source surface(PFSS) and Schatten current sheet (SCS) model [*Arge and Pizzo*, 2000; *Arge et al.*, 2003, 2004; *McGregor et al.*, 2008]. The PFSS model determines the coronal magnetic field out to 2.5 $R_{\odot}$ assuming no volu-

[1]Astronomy Department, Boston University, Boston, Massachusetts, USA.
[2]Kirtland Air Force Base, Albuquerque, New Mexico, USA.
[3]NASA/GSFC, Greenbelt, Maryland, USA.
[4]Space Plasma Physics, Department of Physics, University of New Hampshire, Durham, New Hampshire, USA.

0148-0227/11/2010JA016006

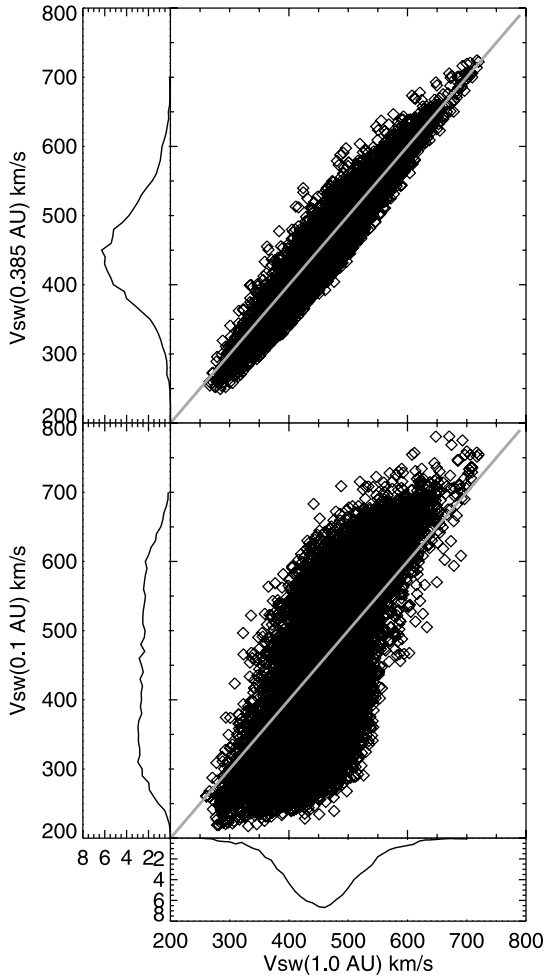

Figure 1. Scatterplots of speeds at two radial distances along solar wind streamlines for 3 years around solar minimum, 1995–1997 (Carrington rotation (CR), 1891–1931). Streamlines are initiated at 1.0 AU at the center of cells at heliographic latitudes of ±6° and ±2° and are traced backward through ENLIL ending at (top) 0.385 AU or (bottom) the inner boundary at 0.1 AU. The horizontal axis shows speeds at 1.0 AU, while the vertical axis shows speeds at 0.385 and 0.1 AU. The grey line indicates no speed change, and it separates solar wind that has accelerated (below the line) from that which has decelerated (above the line). The curve below the scatterplots shows the normalized solar wind speed distribution at 1.0 AU. The curves on the left show the normalized solar wind speed distributions at 0.385 and 0.1 AU.

metric currents [*Schatten et al.*, 1969; *Altschuler and Newkirk*, 1969]. Beyond 2.5 $R_\odot$ the SCS model determines the coronal magnetic field assuming no currents save at the polarity inversion [*Schatten*, 1971]. We use NSO line of sight synoptic magnetograms on the inner boundary to calculate the coronal field out to 21.5 $R_\odot$. Speeds are then calculated on a 21.5 $R_\odot$ sphere using the magnetic flux tube expansion factor [*Wang and Sheeley*, 1990] between 1 and 2.5 $R_\odot$ and the location of the flux tube foot point within an open flux region on the solar surface [*McGregor et al.*, 2011; *Arge et al.*, 2004]. We use the ENLIL solar wind model to propagate the solar wind speeds calculated by the WSA model out into the heliosphere. ENLIL is a 3-D Magnetohydrodynamic heliospheric code that uses a thermal energy equation with $\gamma = 1.5$. At its inner boundary ENLIL uses the radial magnetic field polarity and solar wind speed directly from WSA, calculates the density from an empirical fit to historic Helios observations [*McGregor et al.*, 2011], and calculates temperature by assuming constant thermal pressure. We use an ENLIL grid resolution of 4° in both latitude and longitude and 1.6 solar radii in the radial direction. We focus on a subset of the interval previously validated by *McGregor et al.* [2011], covering both solar minimum (1995–1997) and maximum (1999–2000), and extend the analysis to cover the current solar minimum (2007–2008).

3. Tracing Procedure

[5] In a steady state solution, mapping along magnetic field lines at a single point in time reveals how a plasma parcel evolves as it flows through the heliosphere. This is due to frozen-in conditions in which field lines are passively convected by solar wind flow. We ran the steady state version of the WSA-ENLIL model for 99 Carrington Rotations. These rotations covered 7 years, 3 solar minimum years (1995–1997), 2 years near solar maximum (1999–2000), and 2 years during the current solar minimum (2007–2008). For each rotation we traced the magnetic field using a fourth-order Runga-Kutta method, starting at 1.0 AU at the center of all the cells in the four rows nearest the heliographic equator. The centers of these cells are at −6° , −2° , 2° , and 6° heliographic latitude, spanning the range of heliographic latitudes traversed by the Earth. For each field line tracing we recorded the model solar wind speed at three radial distances, 1.0 AU, 0.385 AU (close to the perihelion distance of the Helios spacecraft) and 0.1 AU (the inner boundary of ENLIL). From the 99 Carrington Rotations we obtained 35,640 individual mappings.

4. Solar Wind Speed Evolution

4.1. Solar Minimum, 1995–1997

[6] Figure 1 shows the evolution of the solar wind speed predicted by the WSA-ENLIL model during the solar minimum years 1995–1997. The two larger panels show scatterplots of the predicted speed at 0.385 AU (top) and at 0.1 AU (bottom) as a function of the speed at 1.0 AU. To the left and below the scatterplots we show normalized curves of the solar wind speed distributions at 1.0 AU (below), 0.385 AU (top left), and 0.1 AU (bottom left). These curves have been scaled to make the labels easier to understand. Figure 1 (top) shows that solar wind speeds do not vary much between 0.385 and 1.0 AU. The grey diagonal line separates the solar wind which has accelerated (below line) and decelerated (above the line). Slight acceleration and deceleration occurs, with a maximum difference in speed on the order of ±50 km/s, but overall the speed at 1.0 AU is a good approximation of the plasma parcel speed at 0.385 AU. Similarly the curves of the normalized speed distributions at 1.0 AU (below) and 0.385 AU (top left) are very similar, though the speed of the peak in the distribution increases a little (~445 km/s to ~460 km/s) showing a slight overall acceleration between 0.385 and 1.0 AU. This is consistent with comparisons of solar wind observations made by Helios and L1 spacecraft which show solar wind speed

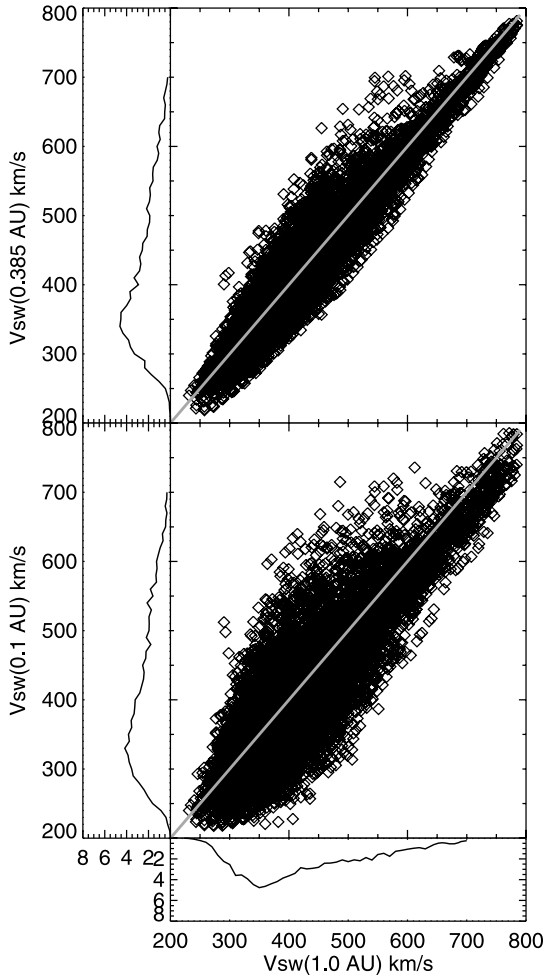

Figure 2. Scatterplots and curves of speeds at two radial distances along solar wind streamlines for 2 years near solar maximum, 1999–2000 (CR, 1945–1975), as in Figure 1.

distributions at 0.3–0.4 AU are similar, but not identical to those seen at 1.0 AU [*McGregor et al.*, 2011].

[7] When predicted speeds at 1.0 AU are compared with those at 0.1 AU (Figure 1, bottom) instead of at 0.385 AU a very different picture emerges. A significant evolution of solar wind speed is evident in Figure 1 (bottom). Solar wind with speeds less than ~330 km/s at 1.0 AU has been accelerated from slower speeds at 0.1 AU (below the diagonal grey line), while most solar wind with speeds greater than 600 km/s at 1.0 AU has been decelerated from higher speeds (above the diagonal grey line). Solar wind with intermediate speeds at 1.0 AU (between 350 km/s and 550 km/s) has been both decelerated and accelerated, with the largest range in initial speeds (speeds at 0.1 AU) occurring for 1.0 AU speeds between 400 and 500 km/s. This means that, for example, solar wind with a speed of 450 km/s at 1.0 AU could have been accelerated up from a minimum speed of 250 km/s or decelerated down from a maximum speed of about 600 km/s. Curves of the solar wind speed distributions for 0.1 AU and 1.0 (Figure 1) also show this difference in initial speed. The distribution at 1.0 AU resembles a Gaussian with a peak at about 450 km/s, while the speed distribution at 0.1 AU (bottom left) is very broad, and flat across an extended range of solar wind speeds.

4.2. Solar Maximum, 1999–2000

[8] Figure 2 shows the radial evolution of the solar wind speed during the 1999–2000 solar maximum years in the same format as Figure 1. The distribution of solar wind speeds at 1.0 AU during 1995–1997 (solar minimum) and 1999–2000 (solar maximum) (bottom speed distributions in Figures 1 and 2, respectively) are very different. During solar maximum the model speed distribution peaks sharply around 350 km/s and has a long tail of faster solar wind speeds, which is distinctly different from the more symmetric Gaussian distribution obtained during 1995–1997. The evolution of solar wind speeds between 1.0 AU and 0.385 AU during solar maximum (Figure 2, top), is slightly greater than during solar minimum with the acceleration and deceleration resulting in maximum speed differences around ±75 km/s. The distribution of solar wind speeds at 0.385 AU (top left) is very similar to that at 1.0 AU (bottom).

[9] Figure 2 (bottom) shows that significant deceleration/acceleration still occurs between 0.1 AU and 1.0 AU during solar maximum, but that the change in speed is not as dramatic as during solar minimum. Solar wind speeds at 1.0 AU between 400–500 km/s still show the greatest variation in original speeds with changes in speed of up to ±150 km/s possible. However, the lower curves in Figure 2 show that the distribution of speeds at 0.1 AU and at 1.0 AU are much more similar to each other at solar maximum than they were at solar minimum. The smaller range of coronal solar wind speeds during solar maximum, and the less steep gradients between different speed flows, not surprisingly lead to a similar but less pronounced evolution in solar wind speed during solar maximum than during solar minimum.

4.3. Solar Minimum, 2007–2008

[10] Figure 3 shows the radial evolution of the solar wind speed during the most recent solar minimum, specifically for

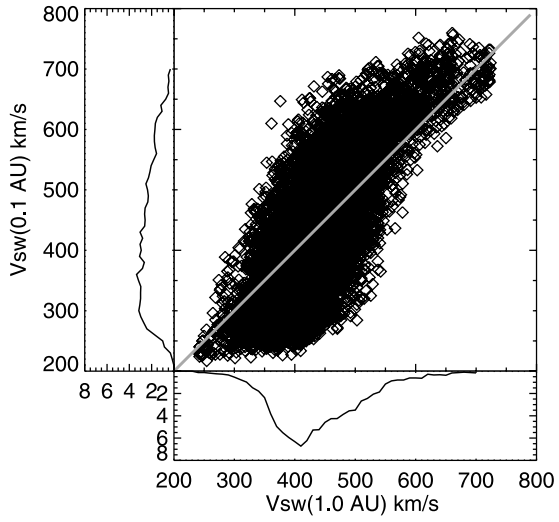

Figure 3. Scatterplot and curves of speeds at 0.1 and 1.0 AU along solar wind streamlines; as in Figure 1 except during 2 years near solar minimum, 2007–2008 (CR, 2052–2078).

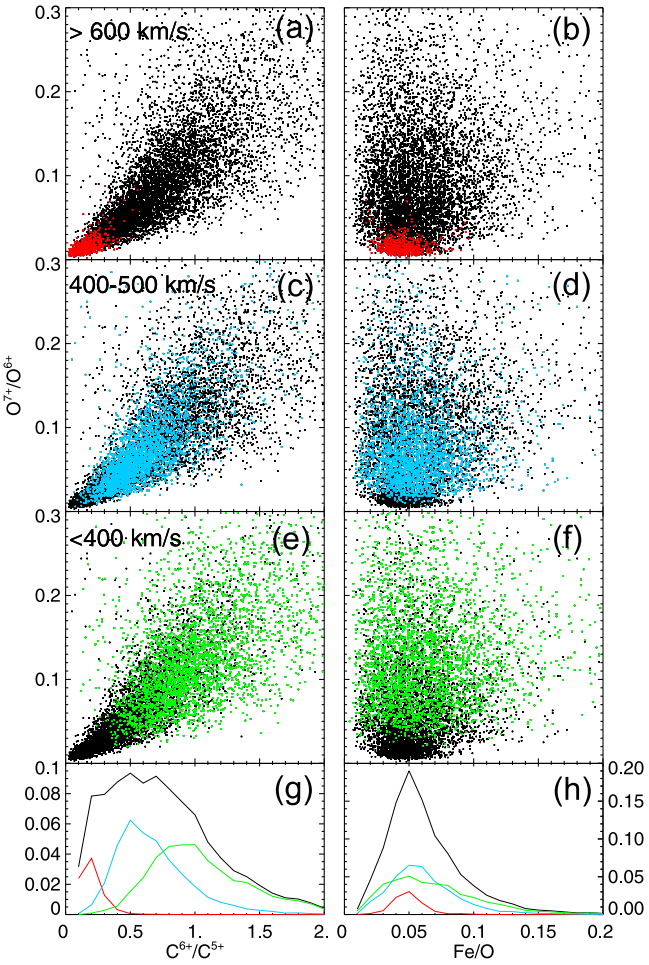

Figure 4. (a-f) Scatterplots showing the O^{7+}/O^{6+} charge state ratio as a function of the (left) C^{6+}/C^{5+} ratio and (right) Fe/O ratio observed by ACE during 2007–2008. Black points denote the entire data set. Colored points indicate specific solar wind speed ranges: red, >600 km/s; blue, 400–500 km/s; and green, <400 km/s. (g and h) Curves showing the distributions of C^{6+}/C^{5+} and Fe/O ratios for the same speed ranges using the same colors.

the years 2007–2008. The scatterplot and curves show how the solar wind speed and the speed distributions change between 0.1 AU (vertical axis) and 1.0 AU (horizontal axis). Similar to during the previous solar minimum (Figure 1), most of the solar wind with speeds greater than 600 km/s at 1.0 AU has decelerated, indicated by their position above the gray line. Most of the solar wind with speeds below 350 km/s at 1.0 AU has accelerated from slower speeds at 0.1 AU. Not only does the scatterplot indicate an evolution of the solar wind similar to that during the previous solar minimum (Figure 1, bottom), but also the peaked and flat distributions of WSA-ENLIL solar wind speeds at 0.1 AU and 1.0 AU (left and bottom, respectively) show a qualitatively similar evolution to the distributions seen in 1995–1997 (Figure 1). The solar wind speed distribution at 1.0 AU in 2007–2008 peaks at about 410 km/s, tapering off at higher speeds, in sharp contrast to the relatively flat solar wind speed distribution in the outer corona at 0.1 AU. Both solar minimum periods showing similar speed evolution within the model suggests that the dramatic evolution of the solar wind speed between the outer corona and 1.0 AU is characteristic of the solar wind during solar minimum conditions, and is not merely a peculiarity of the 1996 solar minimum's uncommonly flat streamer and heliospheric current sheet structure.

5. Solar Wind Composition

[11] In section 4 we showed how the WSA-ENLIL model predicts significant evolution in the solar wind speed between 0.1 AU and 1.0 AU, especially during solar minimum. The lack of plentiful solar wind plasma observations made near the Sun makes it difficult to find direct evidence of the solar wind speed evolution. However, solar wind composition and ionic charge state ratios reflect conditions close to the Sun and can be used to investigate solar wind speed evolution.

[12] Charge states of solar wind ions can be used as a proxy for coronal temperatures as they are not expected to change after they "freeze in" at a few solar radii [*Hefti et al.*, 2000]. In the equilibrium model of *Ko et al.* [1997] the O^{7+}/O^{6+} charge state ratio monotonically increases with increasing electron temperature. So fast solar wind, which has a lower O^{7+}/O^{6+} charge state ratio, originates from regions with lower coronal temperatures (consistent with a coronal hole source) than the slow solar wind which has, on average, a higher O^{7+}/O^{6+} charge state ratio [*Zurbuchen et al.*, 2002]. Likewise the elemental abundance ratios, such as Fe/O, which are determined in the chromosphere, also remain unaffected by the solar wind acceleration that occurs at a higher altitude in the hotter corona. The slow solar wind has an average Fe/O abundance ratio about twice that of the fast solar wind [*Von Steiger et al.*, 2000] indicating differences in the source regions of the two solar wind types.

[13] In section 4 we showed that the WSA-ENLIL model predicts that solar wind observed at 1.0 AU with intermediate speeds (400–500 km/s) can be either accelerated slow wind or decelerated fast wind. So we should expect solar wind observed at 1.0 AU with intermediate speeds to show coronal composition signatures of both the fast and slow solar wind. Since the model suggests that solar wind speed evolution is more pronounced during solar minimum and the 1995–1997 and 2007–2008 minima show similar radial speed evolution, we focus on 2007–2008 solar minimum years when the ACE compositional data is available. We use oxygen and carbon ionic charge state ratios and Fe/O measurements from the SWICS-ACE instrument and solar wind speed measurements from the SWEPAM-ACE instrument at 1 h resolution during the solar minimum years 2007–2008.

[14] Figure 4 shows the O^{7+}/O^{6+} charge state ratio as a function of the C^{6+}/C^{5+} charge state ratio (left) and Fe/O ratio (right) as scatterplots. The black dots show the entire data set while in each panel data from a limited range of solar wind speeds is highlighted in color. Red, blue and green indicate a solar wind speed range of greater than 600 km/s, 400–500 km/s, and less than 400 km/s, respectively. Solar wind speeds greater than 600 km/s were chosen because the model indicates that at 1.0 AU in the equatorial region, solar wind observed above 600 km/s has rarely been accelerated from slower speeds (see Figure 3), therefore speeds greater than 600 km/s should be pristine fast solar wind. Figure 4a shows that solar wind with speeds greater than 600 km/s is confined to a narrow range of both O^{7+}/O^{6+} and C^{6+}/C^{5+} charge state

ratios. This solar wind rarely has an O^{7+}/O^{6+} value greater than 0.05, or a C^{6+}/C^{5+} charge state ratio greater than 0.5. These maximum O^{7+}/O^{6+} and C^{6+}/C^{5+} values correspond to maximum electron temperatures in the coronal source region of 1.23 MK and 1.11 MK, respectively. The C^{6+}/C^{5+} charge state ratio freezes into the solar wind lower in the corona than the O^{7+}/O^{6+} charge state ratio, consistent with the lower temperature indicated above. These results are consistent with the fast solar wind freezing in quickly at very low heights in cool coronal holes.

[15] Figure 3 shows that solar wind with speeds below 400 km/s at 1.0 AU may have had any speed up to 500 km/s at 0.1 AU. Correspondingly, the green points in Figure 4e cover a much broader range in both O^{7+}/O^{6+} and C^{6+}/C^{5+} charge state ratios (and therefore in coronal electron temperatures) but show almost no overlap with the values observed in the fast solar wind (red points). The spread of both O^{7+}/O^{6+} and C^{6+}/C^{5+} charge states is very broad for the slower solar wind, with no one value of O^{7+}/O^{6+} or C^{6+}/C^{5+} by themselves being sufficient to designate the solar wind as slow or fast in origin. For example, exceedingly low values of C^{6+}/C^{5+} (less than 0.2), are observed in the slow solar wind with high (greater than 0.1) O^{7+}/O^{6+} charge state ratios.

[16] Finally, from Figure 3 we see that solar wind having intermediate speeds of 400–500 km/s at 1.0 AU has the broadest range of speeds at 0.1 AU. Correspondingly the blue points in Figure 4c cover the broadest range of charge state ratios. The ionic charge states of the intermediate-speed solar wind overlaps with both the fast and slow populations, the narrow range of O^{7+}/O^{6+} and C^{6+}/C^{5+} values observed in the fast solar wind (red, Figure 4a), as well as the broad range of O^{7+}/O^{6+} and C^{6+}/C^{5+} values observed in the slow solar wind (green, Figure 4e). This is confirmed by the distributions in Figure 4g which show the values of C^{6+}/C^{5+} ratio observed in the three solar wind speed ranges plotted in the corresponding color. The slow solar wind (green) and fast solar wind (red) have almost no overlap in C^{6+}/C^{5+} charge state ratios. What little overlap that does occur in the C^{6+}/C^{5+} distributions is at relatively high O^{7+}/O^{6+} ratios, and is not coincident with the narrow band of small O^{7+}/O^{6+} and C^{6+}/C^{5+} ratios associated with the fast (red) solar wind. In contrast, the distribution of C^{6+}/C^{5+} charge state ratios observed in intermediate-speed solar wind (blue curve) overlaps both the fast and slow distributions, intersecting the fast wind distribution (red) at about half max, and the slow solar wind distribution almost at its peak. This result suggests that intermediate-speed solar wind can originate at coronal electron temperatures consistent with coronal signatures of both fast and slow solar wind, which is consistent with the model results that a large portion of the population of intermediate-speed solar wind is produced by the acceleration and deceleration of slower and faster winds.

[17] Figure 4 (right) shows the O^{7+}/O^{6+} charge state ratio plotted against the Fe/O abundance ratio in the same format as Figure 4 (left). The range of Fe/O abundance ratios observed in the slow solar wind (green) is much greater than the range in the fast solar wind (red) as previously noted by *Von Steiger et al.* [2000], with the fast solar wind confined to values between 0.03 and 0.07, while values in the slow solar wind range from 0.01 to larger than 0.15. In other words, the values of Fe/O ratio observed in the fast solar wind are merely a subset of the values observed in the slow wind. This is clearer in the distributions of Fe/O values for the three speed bins shown in Figure 4h. The slow and intermediate-speed solar wind (green and blue, respectively) have a broad distribution of Fe/O values, encompassing those of the fast solar wind. These broad distributions show that, even though slower solar wind has a higher average value of Fe/O ratio, the Fe/O value of a particular parcel of solar wind cannot be used to indicate its origin as fast or slow wind. Additionally, if the Fe/O abundances are enhanced over photospheric values in the slower solar wind due to wave heating on closed loops as suggested by *Schwadron et al.* [1999] then the coronal source of this wind must be on loops of varying sizes, not only large ones.

6. Summary and Discussion

[18] Analysis of the evolution of the solar wind speed within the WSA-ENLIL model from 0.1 AU to 1.0 AU shows that the evolution of the speed of a single plasma parcel in the solar wind can be much larger than is usually assumed. Most of the solar wind speed change occurs within 0.385 AU of the Sun, although it is not limited to this region; evolution still occurs between 0.385 AU and 1.0 AU. This finding is consistent with those from the Helios mission [*Rosenbauer et al.*, 1977; *Schwenn et al.*, 1978] which showed longitudinal speed gradients ($dV_r/d\phi$) are much steeper at 0.3 AU than they are at 1.0 AU, implying some mechanism that reduces the longitudinal speed gradients as plasma travels out to 1.0 AU. These same mechanisms may well operate within 0.3 AU, where the longitudinal solar wind speed gradients are even steeper, causing most of the solar wind speed evolution to occur closer to the Sun. *Pizzo* [1980], using 3-D MHD simulations, showed that pressure gradients arising from the stream interactions drive nonradial flows which help offset the kinematic steepening. The nonradial flows, although small in comparison to the radial flows (no more than 10%), allow the plasma to slip laterally. This process also has the effect of accelerating or decelerating adjacent flows as the plasma meridionally slips to different latitudes within the models.

[19] The evolution from initial solar wind speeds at 0.1 AU to speeds at 1.0 AU is more pronounced during solar minimum than during solar maximum. This could be because the initial velocity field at 0.1 AU during solar minimum has a more well-defined simple structure with a greater range of speeds and steeper gradients than during solar maximum. Solar wind with speeds in the 400–500 km/s range at 1.0 AU is the most likely to have undergone significant change in speed, which means that solar wind in this speed range probably had a different speed in the inner heliosphere. Thus care must be taken in interpreting solar wind observations at 1.0 AU based simply on its current speed (fast versus slow), especially if those speeds are "intermediate speeds" of 400–500 km/s.

[20] Observations of the ionic charge state ratios in intermediate-speed solar wind are consistent with this picture of acceleration and deceleration from slower and faster speeds during solar minimum. Although the charge state analysis presented here focuses on solar minimum, a similar mixture of slow and fast wind signatures should be evident in intermediate-speed solar wind during solar maximum. *Wang and Sheeley* [2003] found solar wind speeds slower than might be expected based on their ionic charge state ratios during solar

maximum, citing the interaction with surrounding slow solar wind as the cause for the deceleration.

[21] We found that fast solar wind (>600 km/s) had a very narrow range of both O^{7+}/O^{6+} and C^{6+}/C^{5+} charge state ratios. Previous studies have used the O^{7+}/O^{6+} charge state ratio to determine the solar wind origin [*Zhao et al.*, 2009; *Zurbuchen et al.*, 2002]. *Zhao et al.* [2009] uses the O^{7+}/O^{6+} ratio to separate the solar wind into coronal hole, noncoronal hole, and ICME sources. They use a O^{7+}/O^{6+} ratio of 0.145 to separate between coronal hole and noncoronal hole sources. We can see from Figure 4 that this cutoff value is well outside the narrow range of O^{7+}/O^{6+} and C^{6+}/C^{5+} ratios observed in the fast solar wind. The *Zurbuchen et al.* [2002] cutoff ratio value of 0.1 is also outside the range observed in the fast solar wind, but this may be due to our solar wind speed cutoff used of $V_{SW} > 600$ km/s, which is a bit high. However, the *Zurbuchen et al.* [2002] cutoff ratio of 0.1 also produces a wide range of C^{6+}/C^{5+} values, some of which are more consistent with the slower solar wind. A better approach might be to take into account both the O^{7+}/O^{6+} and C^{6+}/C^{5+} ratios, applying cutoffs to each species, when attempting to determine coronal sources directly from observations.

[22] When analyzing the solar wind for a particular time interval, structure seen in the O^{7+}/O^{6+} ratio is not seen in the solar wind speed or magnetic field [*Zurbuchen et al.*, 2000; *Hefti et al.*, 2000], indicating not only significant evolution of the solar wind speed as it propagates through the heliosphere, but also the discrete nature of the coronal sources. As solar wind streams evolve, especially those observed with intermediate speeds (400–500 km/s), they can lose the speed signature of their source regions, and only the compositional data remains as a true signature of their origin. Understanding the radial evolution of the solar wind can help us decouple the evolution in speed from the composition, and put constraints on solar wind models. The compositional observations shown here show that the intermediate-speed solar wind (400–500 km/s) represents a mix of what was originally fast and slow wind. This, in turn, implies that solar wind is more bimodal (with fast and slow wind states) near 0.1 AU than 1.0 AU.

[23] **Acknowledgments.** This work was supported by CISM, which is funded by the STC Program of the National Science Foundation under cooperative agreement ATM-0120950. I benefited from the availability of ACE SWICS (PI: T. Zurbuchan) and SWEPAM (PI: D. McComas) data. We thank the National Solar Observatory for providing access to their synoptic magnetogram data sets.

[24] Philippa Browning thanks Merav Opher and another reviewer for their assistance in evaluating this paper.

References

Altschuler, M. A., and G. Newkirk (1969), Magnetic fields and the structure of the solar corona, *Sol. Phys.*, *9*, 131–149.

Arge, C. N., and V. J. Pizzo (2000), Improvement in the prediction of solar wind conditions using near-real time solar magnetic field updates, *J. Geophys. Res.*, *105*(A5), 10,465–10,479.

Arge, C. N., D. Odstrcil, V. J. Pizzo, and L. R. Mayer (2003), Improved method for specifying solar wind speed near the Sun, in *Solar Wind Ten*, edited by M. Velli, R. Bruno, and F. Malara, *AIP Conf. Proc.*, *679*, 190–193.

Arge, C. N., D. O. J. G. Luhmann, C. J. Schrijver, and Y. Li (2004), Stream structure and coronal sources of the solar wind during May 12th, 1997 CME, *J. Atmos. Sol. Terr. Phys.*, *66*, 1295–1309.

Hefti, S., H. Grunwaldt, P. Bochsler, and M. R. Aellig (2000), Oxygen freeze-in temperatures measured with SOHO/CELIAS/CTOF, *J. Geophys. Res.*, *105*(A5), 10,527–10,536.

Ko, Y.-K., L. A. Fisk, J. Geiss, G. Gloeckler, and M. Guhathakurta (1997), An empirical study of the electron temperature and heavy ion velocities in the south polar coronal hole, *Sol. Phys.*, *171*, 345–361.

McComas, D. J., H. A. Elliot, J. T. Gosling, D. B. Reisenfeld, R. M. Skoug, B. E. Goldstein, M. Neugebauer, and A. Balogh (2002), Ulysses' second fast-latitude scan: Complexity near solar maximum and the reformation of polar coronal holes, *Geophys. Res. Lett.*, *29*(9), 1290, doi:10.1029/2001GL014164.

McGregor, S., W. Hughes, C. Arge, and M. Owens (2008), Analysis of the magnetic field discontinuity at the potential field source surface and Schatten Current Sheet interface in the Wang-Sheeley-Arge model, *J. Geophys. Res.*, *113*, A08112, doi:10.1029/2007JA012330.

McGregor, S. L., W. J. Hughes, C. N. Arge, M. J. Owens, and D. Odstrcil (2011), The distribution of solar wind speeds during solar minimum: Calibration for numerical solar wind modeling constraints on the source of the slow solar wind, *J. Geophys. Res.*, *116*, A03101, doi:10.1029/2010JA015881.

Odstrcil, D. (2003), Modeling 3-D solar wind structure, *Adv. Space Res.*, *32*(4), 497–506.

Owens, M. J., H. E. Spence, S. L. McGregor, W. J. Hughes, C. N. Arge, P. Riley, J. A. Linker, and D. Odstrcil (2008), Metrics for solar wind prediction models: Comparison of empirical, hybrid, and physics-based schemes with 8 years of L1 observations, *Space Weather*, *6*, S08001, doi:10.1029/2007SW000380.

Pizzo, V. J. (1980), A three-dimensional model of corotating streams in the solar wind: 2. Hydrodynamic streams, *J. Geophys. Res.*, *85*(A2), 727–743.

Rosenbauer, H., R. Schwenn, E. Marsch, B. Meyer, H. Miggenrieder, M. Montgomery, K. Mühlhäuser, W. Pilipp, W. Voges, and S. M. Zink (1977), A survey on initial results of the HELIOS plasma experiment, *J. Geophys.*, *42*(6), 561–580.

Schatten, K. H. (1971), Current sheet magnetic model for the solar corona, *Cosmic Electrodyn.*, *2*, 232–245.

Schatten, K. H., J. M. Wilcox, and N. F. Ness (1969), A model of interplanetary and coronal magnetic fields, *Sol. Phys.*, *6*, 442–455.

Schwadron, N. A., L. A. Fisk, and T. H. Zurbuchen (1999), Elemental fractionation in the slow solar wind, *Astrophys. J.*, *521*, 859–867.

Schwenn, R., M. D. Montgomery, H. Rosenbauer, H. Miggenrieder, K. H. Muhlhauser, S. J. Bame, W. C. Feldman, and R. T. Hansen (1978), Direct observation of the latitudinal extent of a high-speed stream in the solar wind, *J. Geophys. Res.*, *83*(A3), 1011–1017.

Von Steiger, R., N. A. Schwadron, L. A. Fisk, J. Geiss, G. Gloeckler, S. Hefti, B. Wilken, R. F. Wimmer-Schweingruber, and T. H. Zurbuchen (2000), Composition of quasi-stationary solar wind flows from Ulysses/Solar Wind Ion Composition Spectrometer, *J. Geophys. Res.*, *105*(A12), 27,217–27,238.

Wang, Y. M., and N. R. Sheeley (1990), Solar wind speed and coronal flux-tube expansion, *Astrophys. J.*, *355*, 726–732.

Wang, Y. M., and N. R. Sheeley (2003), The solar wind and its magnetic sources at sunspot maximum, *Astrophys. J.*, *587*, 818–822.

Zhao, L., T. H. Zurbuchen, and L. A. Fisk (2009), Global distribution of the solar wind during solar cycle 23: ACE observations, *Geophys. Res. Lett.*, *36*, L14104, doi:10.1029/2009GL039181.

Zurbuchen, T. H., S. Hefti, L. A. Fisk, G. Gloekler, and N. A. Schwadron (2000), Magnetic structure of the slow solar wind: Constraints from compositional data, *J. Geophys. Res.*, *105*(A8), 18,327–18,336.

Zurbuchen, T. H., L. A. Fisk, G. Gloeckler, and R. Von Steiger (2002), The solar wind composition throughout the solar cycle: A continuum of dynamic states, *Geophys. Res. Lett.*, *29*(9), 1352, doi:10.1029/2001GL013946.

C. N. Arge, AFRL/RVBXS, Space Vehicles Directorate, Kirtland Air Force Base, 3550 Aberdeen Ave. SE, Albuquerque, NM 87117-5776, USA.

W. J. Hughes and S. L. McGregor, Astronomy Department, Boston University, Boston, MA 02215, USA. (slmic@bu.edu)

D. Odstrcil, NASA/GSFC, Mail Code 674, Greenbelt, MD 20771, USA.

N. A. Schwadron, Space Plasma Physics, Department of Physics, University of New Hampshire, Durham, NH 03824, USA.